A Wideband Circularly Polarized Antenna Based on Anisotropic Metamaterial

Quan-Wei Lin, *Member, IEEE*, Shaker Alkaraki, *Member, IEEE*, Hang Wong, *Senior Member, IEEE*, and James Kelly, *Member, IEEE*

***Abstract*—This paper presents a novel circularly- polarized (CP) antenna based on an anisotropic metamaterial. The antenna is capable of performing linear-to-circular polarization conversion over a wideband of frequencies in the X-band (8-12GHz). The proposed antenna was constructed from a metamaterial-based polarizer mounted above the aperture of a rectangular waveguide. The polarizer was oriented at 45 degrees to E-plane of the waveguide. The proposed polarizer is composed of multiple metamaterial layers. The unit cell of the proposed polarizer consists of a single dielectric slab incorporating a series of rectangular split ring resonators that are printed on both sides of the slab. Impedance matching layers (IML) are introduced to enhance the Axial-ratio (AR) bandwidth. The polarizer has a low profile in terms of electrical length (thickness of 0.41 λ_0, where λ_0 is the free-space wavelength at 10.5 GHz). A full-wave electromagnetic simulator was used to verify the anisotropic characteristics of the unit cell. This was achieved by showing that the metamaterial exhibits two different refractive indices along the orthogonal components of the incident electric field. The prototype of the proposed design is fabricated and measured to validate the performance. The measured results agree with the simulated ones and demonstrated a wide impedance bandwidth of 62.4% ranging from 7.08 GHz to 13.5 GHz with a 3dB AR bandwidth of 29.9% (9.25-12.5 GHz).**

***Index Terms*—Anisotropic material, CP antenna, circular polarization, polarizer, metamaterial, refractive index**

I. Introduction

THE polarization of an electromagnetic wave plays a crucial role in determining the effectiveness with which the resources of a wireless communication system can be used. For example, compared with linear polarization (LP), circular polarization (CP) offers a range of significant advantage, including: low polarization mismatch, lower multipath, and resilience to phase rotation in the upper atmosphere of the earth (e.g., due to faraday rotation) [1-3]. For this reason, CP antennas are more attractive than linearly polarized (LP) antennas for applications, such as satellite communication and GPS navigation [4], imaging [5], and radar [6]. The handedness of CP is converted on reflection from a metallic surface. In radar applications, therefore a CP wave is a good way to distinguish the transmitted wave from the received wave using the handedness of CP [2].

A variety of CP radiators, including antenna and array, have been reported in the literature. These include the: cross-dipole antenna [7], helix antenna [8], spiral antenna [9], microstrip patch antenna [10], and dielectric resonator antenna (DRA) [11]. Wire antennas are a popular choice for generating CP radiation [7-9] because they have a simple structure, high polarization purity, and wide operating bandwidth. However, their performance is highly sensitive to fabrication errors, and such designs tend to have a high profile, which makes them unsuitable for use within modern systems requiring compact antennas. The microstrip patch antenna and dielectric resonator antenna (DRA) [10-11] are also popular choices whose advantages include ease of fabrication using PCB techniques, additional degrees of freedom in the feeding network, and robustness. The resonant frequency of the microstrip patch and DRA are determined by their shape and dielectric permittivity. Consequently, two orthogonal modes with a 90° phase difference can be excited by introducing asymmetries into the geometry of the resonator or by employing a feed network that creates two sources of excitation separated by a phase difference of 90°. However, the significant drawback of such approaches is that the resulting AR bandwidth tends to be narrow.

An alternative approach for generating CP waves is to use an LP-CP polarizer fed by an LP radiator. Frequency selective surfaces (FSS) have frequently been employed for this purpose [12-14]. When employing an FSS for this purpose, we generally require an incident wave orientated at 45° to the co-ordinate axes. The FSS is built from an array of metallic patterned unit cells, such as meandering lines [12], crosses [13], or split rings [14]. These elements split the incoming wave into two components having a 90° phase difference and the result is a CP wave. FSS provide a flexible way to control the transmission characteristics by varying the geometry of the unit cell. However, the FSS is based around resonant elements which operate over a narrow range of frequencies. This leads to relatively narrow AR bandwidth together with high insertion losses. A dielectric polarizer based on an artificial anisotropic material has been reported in the literature, and it showed good

This work was supported in part by the Research Grants Council of the Hong Kong SAR, China (Project No. GRF project 11210621), the Guangdong Provincial Department of Science and Technology, China (Project No. 2020B1212030002), and the National Natural Science Foundation of China (Grand 62071408).

Shaker Alkaraki and James Kelly are with the School of Electronic Engineering and Computer Science, Queen Mary University of London, London E1 4NS, U.K.

Quan Wei Lin and Hang Wong are with The State Key Laboratory of Terahertz Millimeter Waves, Department of Electrical Engineering, City University of Hong Kong, Hong Kong (e-mail: hang.wong@cityu.edu.hk).

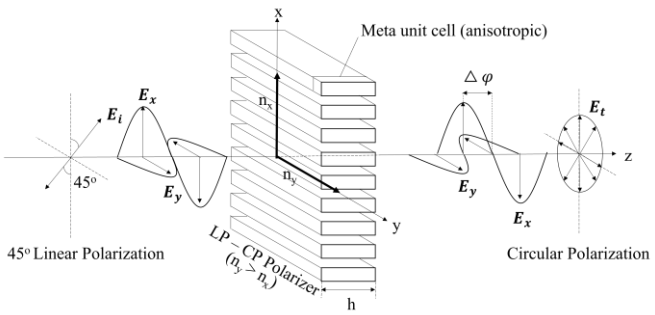

Fig. 1. Working principle of a polarizer based on anisotropic metamaterials.

performance over a broadband of frequencies [15]. The dielectric polarizer consists of a series of dielectric slabs separated by equal gaps. Due to the introduction of the air gap, such polarizer is regarded as the composite material and it is able to realize a range of different effective permittivity along its orthogonal axes. The effective permittivity along each corresponding axes are determined by the ratio of filling factor of dielectric material to air. The necessary conditions for obtaining CP polarization (i.e., 90° phase difference and equal magnitude) can be obtained by optimizing the length of the air gap separating the dielectric slabs. This approach, therefore addresses the limitations of the FSS based polarizer. However, the effective permittivity is limited by the dielectric constant of the chosen dielectric substrate. Also, this kind of polarizer tends to have bulky size compared with FSS.

This paper presents a novel wideband circularly polarized antenna based on anisotropic metamaterial. It consists of a series of rectangular metallic split ring resonators mounted on the dielectric slabs. The unit cell exhibits different refractive indices along the two orthogonal-axes. The parameters of the unit cells are optimized to fulfil the required 90° phase difference of the outcoming waves in two orthogonal polarizations for generating a CP wave. Besides, impedance matching layers are proposed to reduce the insertion loss of the outcoming waves. To validate the performance, the proposed polarizer is fed by an open-ended rectangular waveguide and the assembled prototype is fabricated and measured.

This paper is organized as follows. Section II introduces the methodology employed to design the anisotropic metamaterial LP-CP polarizer. Section III presents the design and analysis of the unit cell as well as the overall structure. Section IV, presents the simulated and measured results for the proposed CP antenna. Finally, conclusions are drawn in Section V.

II. Methodology of CP Antenna Based on an Anisotropic Metamaterial

A. Realization of Circular Polarization (CP)

Fig. 1 illustrates the basic working principle of the polarizer composed of anisotropic metamaterials. The proposed polarizer is regarded as the birefringent that demonstrates two different refractive indices (n_x & n_y) along two mutually orthogonal directions (x- & y-axis shown in Fig. 1). The polarization of the incident wave (E_i) is orientated at 45° with respect to the x-axis, while the propagation direction is along the z-axis. The

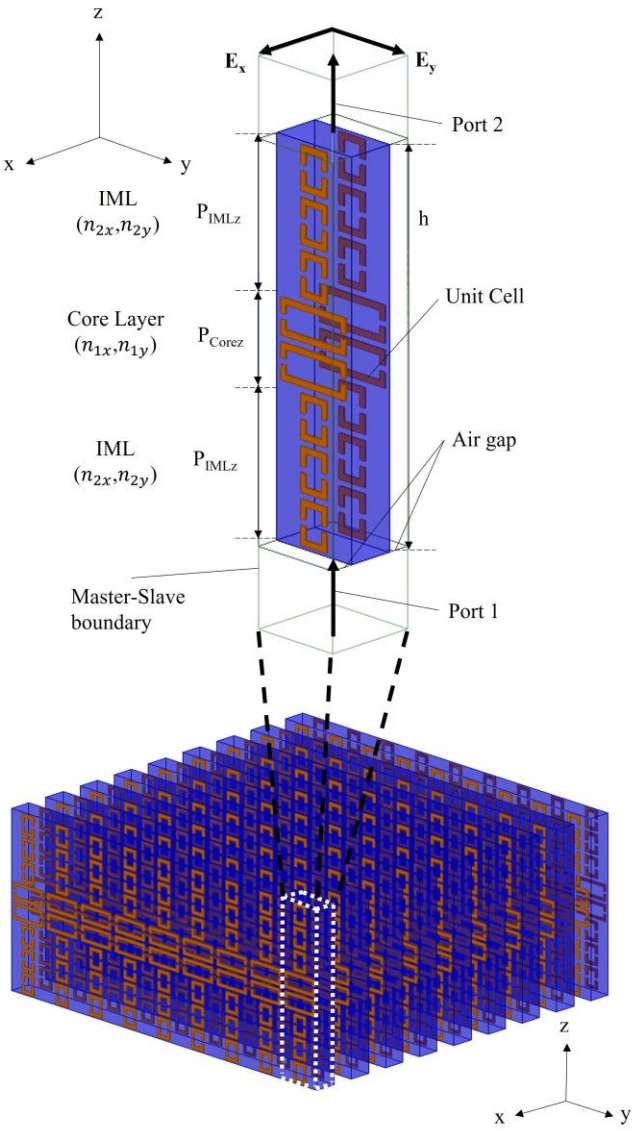

Fig. 2. Schematic of the proposed metamaterial unit cell.

resolved vector can be decomposed into two orthogonally polarized components, namely: E_x and E_y. Since the relationship of refractive indices is specified as $n_y > n_x$, E_x will propagate through the polarizer with a velocity of c/n_x faster than E_y with a velocity of c/n_y. For the thickness of the proposed polarizer (h), the phase changes of two orthogonal waves through the polarizer are given as follows:

$$\begin{cases} \varphi_x = k_x h = \dfrac{2\pi n_x}{\lambda_0} h \\ \varphi_y = k_y h = \dfrac{2\pi n_y}{\lambda_0} h \end{cases} \quad (1)$$

where k_x and k_y are the wave vector of the x- and y-component of E-field respectively, λ is the free space wavelength. This yields a phase difference ($\Delta\varphi$) between the two orthogonally polarized components [16],

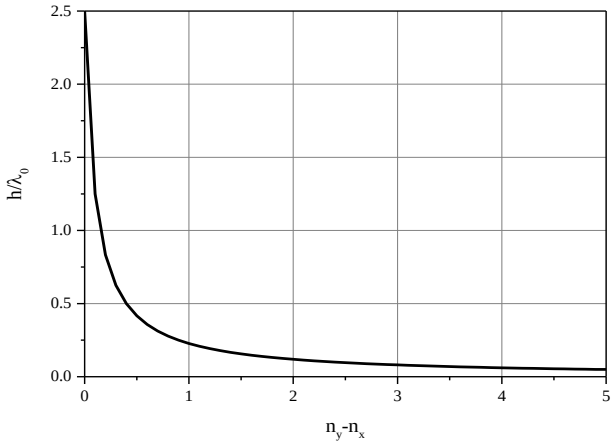

Fig. 3. Calculated height of the polarizer versus refractive-index differences for the requirement of generating CP wave.

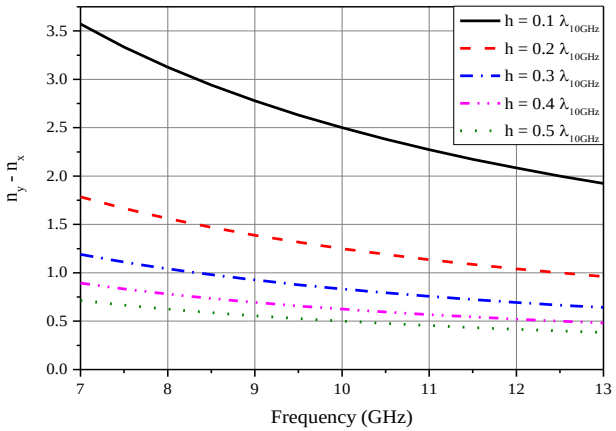

Fig. 4. Refractive-index differences versus frequencies at different heights of polarizer.

$$\Delta\varphi = \frac{2\pi\left|n_y - n_x\right|h}{\lambda_0} = \frac{2\pi\Delta n h}{\lambda_0} \tag{2}$$

where h is the height of the unit cell, n_x and n_y are the refractive indices in x- and y- polarization, Δn is the difference between n_x and n_y, and λ_0 is the free-space wavelength at operating frequency. In order to convert the incident LP wave into CP wave, the phase difference $\Delta\varphi$, should be -90° for left-handed circular polarization (LHCP) or 90° for right-handed circular polarization (RHCP). Fig. 3 plots the normalized height (h) of the unit cell in the wavelength as a function of the refractive-index difference Δn with $\Delta\varphi$=90° derived from (2). It reveals that the height of the metamaterial is inversely proportional to the refractive-index difference. This indicates that the refractive-index difference of the polarizer should be increased in order to reduce the height of the polarizer.

B. Wideband performance

However, simply increasing refractive-index difference may not be an optimal way to realize a CP polarizer because it will compromise its bandwidth. Fig. 4 plots the calculated refractive-index differences for $\Delta\varphi$=90°, as a function of frequency for different heights of the polarizer. It can be observed that the calculated refractive-index difference decreases as the frequency increases. It can also be observed, from Fig. 4, that the variation in the refractive-index difference, as a function of frequency, increases as the thickness of the unit cell reduces. However, the intrinsic characteristic of metamaterials is that the refractive-index difference will increase or keep constant as the frequency increases. Therefore, the impedance bandwidth is limited when the refractive-index difference is increased to reduce the height of the polarizer. We need to compromise the bandwidth and the height of the polarizer.

C. Impedance Matching

The refractive index of a material is given by the well-known formula in (3).

$$n = \sqrt{\varepsilon_r \mu_r} \tag{3}$$

where ε_r and μ_r are the relative permittivity and relative permeability of the material in question. For most materials (except ferrites) μ_r = 1 and thus the formula for the refractive index can be further simplified to $n = \sqrt{\varepsilon_r}$. The wave impedance within the metamaterial is given by (3).

$$\eta = \eta_0 \frac{\sqrt{\mu_r}}{\sqrt{\varepsilon_r}} = \frac{\eta_0}{n} \tag{4}$$

where: $\eta_0 = \frac{\sqrt{\mu_0}}{\sqrt{\varepsilon_0}}$ is the characteristic impedance of free-space.

According to (3) and (4), the refractive index for a metamaterial may result in an impedance mismatching at the interface between air and metamaterial. In turn this would increase the level of insertion loss and distortion experienced by the two orthogonally polarized incident waves, thus degrading the purity of the transmitted CP wave. When encountering the high refractive index for a metamaterial (n > 2), Impedance matching layers (IMLs) are introduced, above and below the core layer, as shown in Fig. 2, to address this issue. The impedance matching layer serves as a quarter wavelength transformer whose wave impedance is given by (5) which represents the geometrical mean of the wave impedance of free-space and that of the core layer [17].

$$\eta_2 = \sqrt{\eta_0 \eta_1} \tag{5}$$

where: η_2 and η_1 denote the wave impedance of the IML and the core layer, respectively. The refractive index of the IML is given by,

$$n_2 = \sqrt{n_1} \tag{6}$$

where: n_2 and n_1, are the refractive indices for the IML and core layer, respectively.

The relationship between the thicknesses of the IML and core layer (denoted as P_{IMLz} and P_{Corez}) is given by,

$$2P_{IMLz} n_2 + P_{Corez} n_1 = hn \tag{7}$$

From (6) & (7), we have

$$2P_{IMLz}\sqrt{n_1} + P_{Corez} n_1 = hn \tag{8}$$

where: h and n represent the overall thickness and refractive index of the proposed metamaterial, respectively. (8) regards the composition of the IML and core layer as the equivalent

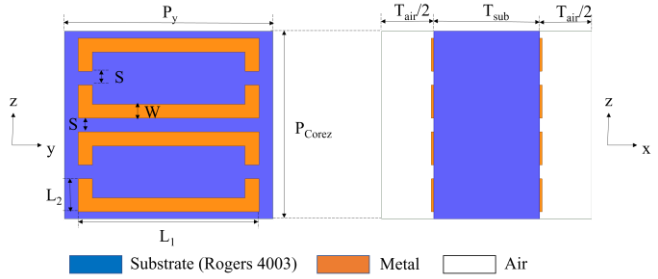

Fig. 5. Configuration of core layer for the proposed anisotropic metamaterial unit cell. The parameters are $P_y = 3$, $P_{CoreZ} = 2.7$, $L_1 = 2.6$, $L_2 = 0.475$, $S = 0.2$, $W = 0.2$, $T_{air} = 0.75$, $T_{sub} = 1.524$ (all in mm).

medium for analysis of the height of the unit cell for corresponding layers. The required height of the IML and the core layer P_{IMLz} and P_{Corez} can be determined with the obtained values of the refractive index of the core layer (n_{1y}), the effective index of the overall polarizer (n_y), and the length of the overall polarizer (h).

III. Design of CP Polarizer Based on Anisotropic Metamaterial

As introduced in Section II-C, the proposed unit cell is a three-layer stacked configuration, incorporating the core layer sandwiched between two layers of IML. Master-slave boundary condition were assigned around the enclosure of the simulated model. This effectively produces a periodic structure with floquet port excitation along the x- and y-axis directions and enables us to extract the scattering response of the proposed unit cell. The refractive index of the unit cell was retrieved from the scattering response using,

$$n = \frac{1}{kd}\cos^{-1}\left(\frac{1}{2S_{21}}\left(1 - S_{11}^2 + S_{21}^2\right)\right) \quad (9)$$

where k is the propagation constant, and d is the thickness of a single layer. It is worth noting that (9) is only applicable to structures which are symmetric along the direction of wave propagation [18]. The following section presents details relating to the design and performance of each layer of the unit cell.

A. Core Layer Unit Cell Design

Fig. 5 illustrates the structure of the core layer of the anisotropic unit cell. It comprises two rectangular split ring resonators printed symmetrically on both sides of a single-layer substrate. The substrate is formed from Rogers 4003C ($\varepsilon_r = 3.55$, $\tan\delta = 0.0027$) with a thickness of $T_{sub} = 1.524$mm. Because the finalized design of the proposed polarizer is by duplicating the unit cell in x-axis with the air gap of 1.5 mm, and duplicating it in y-axis. Therefore, two air gaps with thickness of 0.75 mm were introduced in the unit cell simulation to imitate the EM wave passing through the periodic metamaterial. Fig. 6 shows the simulated refractive indices of the proposed unit cell for core layer, calculated from (9), with excitations along the x- and y-polarizations. It can be observed that the retrieved refractive indices for both the x- and y-polarizations are stable over the frequency range. It is indicated that the structure is suitable for realizing the wideband performance when the material height is 0.4 λ_0 (refer to Fig. 4). Furthermore, the imaginary parts of the refractive indices are close to zero over the operating frequency band, indicating that there is little attenuation of EM wave as it passes through the unit cell.

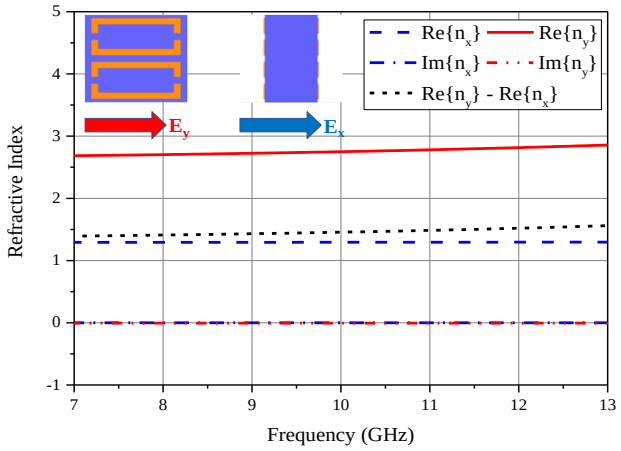

Fig. 6. Simulated refractive indices for core layer unit cell in two orthogonal polarizations.

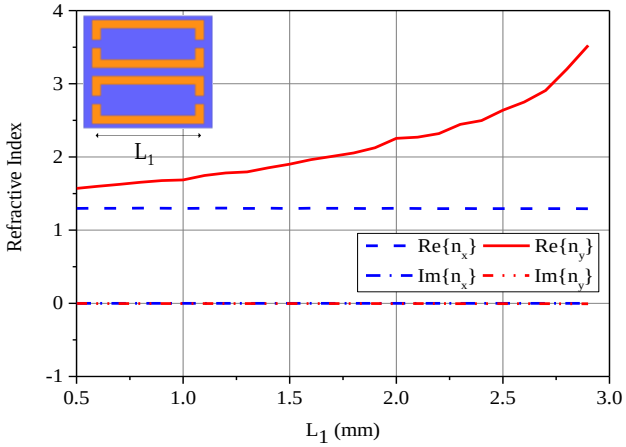

Fig. 7. Simulated refractive indcies of core layer unit cell for different values of L_1 at 10 GHz.

Fig. 7 shows the result of a parametric study on the length of rectangular split ring resonator (L_1). The study was conducted at 10 GHz by changing L_1 while the other parameters remained unchanged. It can be seen that lengthening L_1 in the y-axis direction can increase the refractive index of the unit cell along y-axis. By varying L_1 from 0.5 mm to 2.9 mm, the refractive-index values obtained in the y-polarization range from 1.57 to 3.52. On the other hand, a constant refractive index in x-polarization is realized in 1.29 over the variation of L_1. The key parameter L_1 provided a degree of freedom to manipulate the refractive index in y-polarization while that in x-polarization remains unchanged. To meet the requirement for generating CP wave, the required refractive-index difference derived from (2) can be achieved by independently controlling the refractive index along y-axis.,

B. Impedance Matching Layer (IML) Unit Cell Design

As mentioned in Section II-C, the IML acts as the quarter-wavelength transformer which is used to match the

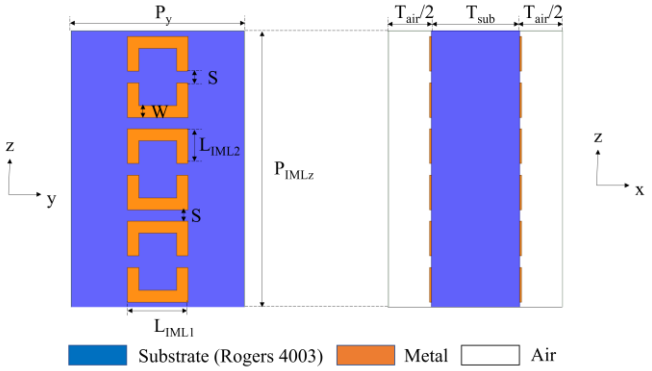

Fig. 8. Configuration of impedance matching layer for the proposed anisotropic metamaterial unit cell. The parameters are P_y = 3, P_{IMLZ} = 4.8, L_{IML1} = 1.05, L_{IML2} = 0.6, S = 0.2, W = 0.2, T_{air} = 0.75, T_{sub} = 1.524 (all in mm).

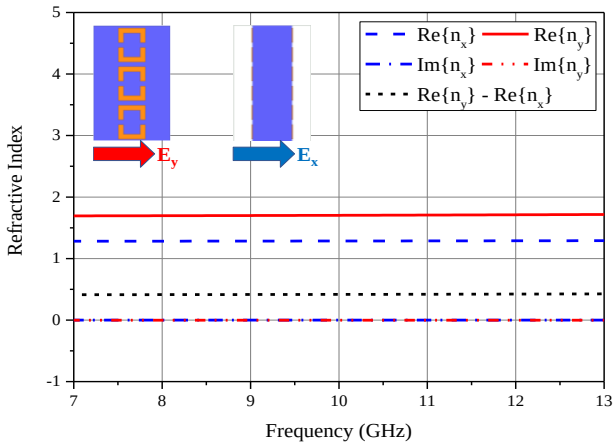

Fig. 9. Simulated refractive indices for IML unit cell in two orthogonal polarizations.

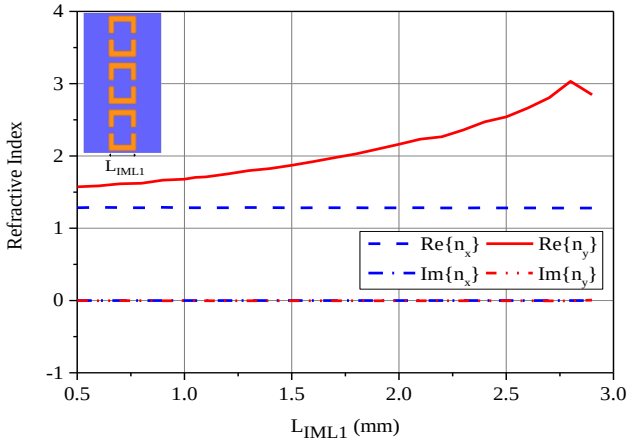

Fig. 10. Simulated refractive indices of IML unit cell for different values of L_{IML1} at 10 GHz.

impedance of free-space to that of the core layer. In order to achieve this, the required refractive index of IML is set to a lower value than that of the core layer according to (6). As shown in Fig. 8, the unit cell for the IML employs the same substrate material as that for the core layer. The unit cell for the IML incorporates three rectangular split ring resonators which are mounted on both sides of the substrate. The same design of

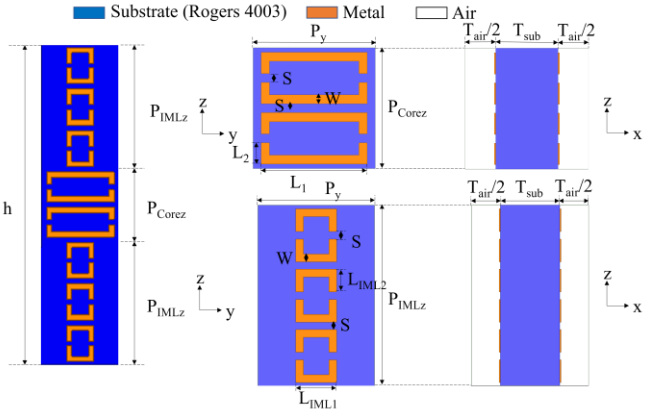

Fig. 11. Configuration of the proposed metamaterial unit cell.

TABLE I
PARAMETERS FOR PROPOSED POLARIZER BASED ON META-MATERIAL

Parameters	H	P_y	P_{CoreZ}	P_{ImlZ}	S	W
Value (mm)	12.3	3	2.7	4.8	0.2	0.2
Parameters	L_1	L_2	L_{Iml1}	L_{Iml2}	T_{Sub}	T_{Air}
Value (mm)	2.6	0.475	1.05	0.6	1.524	0.75

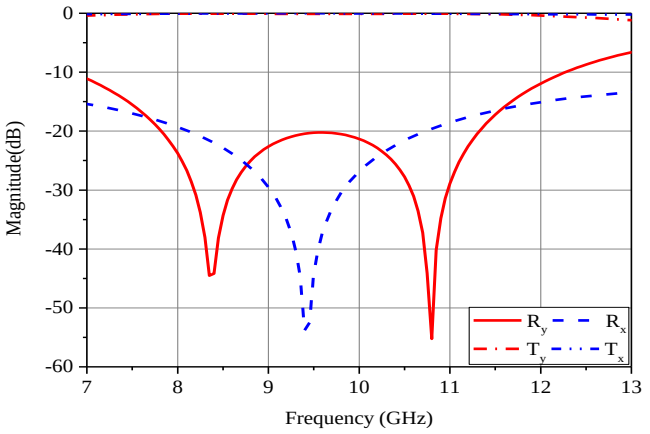

Fig. 12. Simulated reflection coefficient and transmission coefficient of the proposed unit cell in two orthogonal polarizations.

split ring resonator is employed within both the core layer and the IML. However, the split ring resonators employed within the IML are smaller than those used within the core layer. Specifically, their length (L_{IML1}) is shorter. In this way it is possible to obtain a lower refractive index for the IML over the range of frequencies, as shown in Fig. 9. It can be seen that both refractive indices along the x- and y-axes are approximately equivalent to the square root of that of the core layer, which meets the requirement for IML. Furthermore, the imaginary part of the refractive indices along both polarizations remains zero. Moreover, the refractive-index difference between the x- and y-axis remains constant over the frequency range.

Compared with the core layer unit cell, a parametric study on the length (L_{IML1}) of the split ring resonator for IML is also conducted Fig. 10 illustrates the variation of the refractive indices as a function of L_{IML1}. When the L_{IML1} is increased from

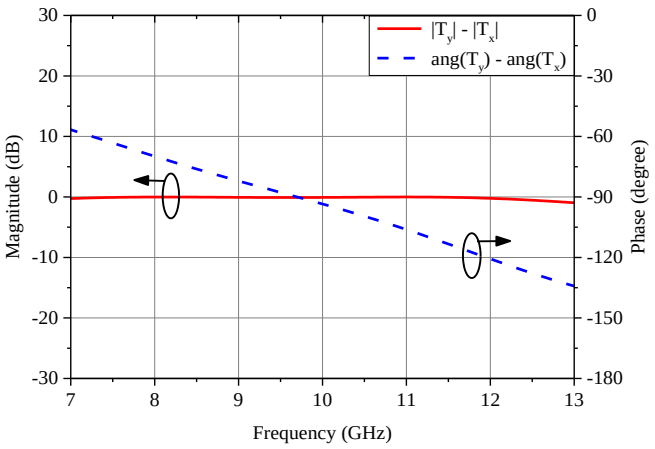

Fig. 13. Magnitude and phase differences between two orthogonal polarizations.

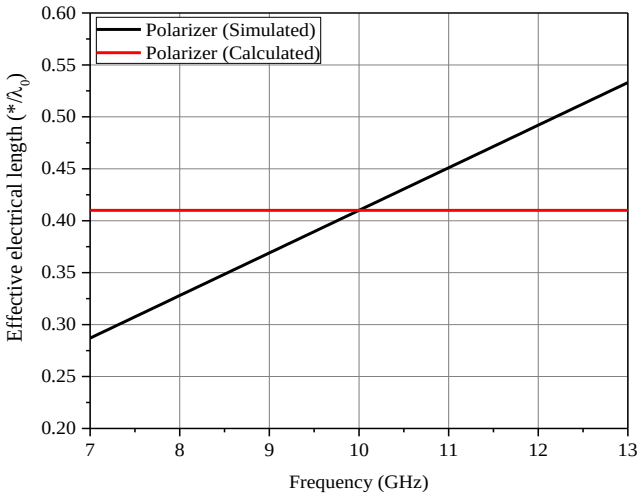

Fig. 14. Effective electrical length of polarizer in y-polarizations over the frequency range.

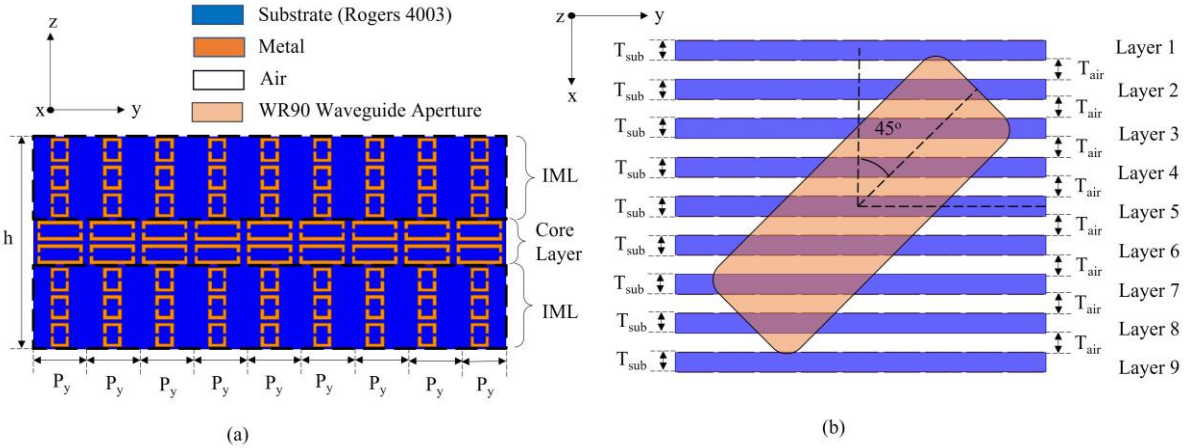

Fig. 15. Configuration of the proposed anisotropic metamaterial-based polarizer (a) front view, and (b) top view.

0.5 mm to 2.9 mm, the refractive index along the y-axis varies from 1.57 to 3.03. Correspondingly, the refractive index along the x-axis remains constant at 1.28. This reveals the way to optimize the L_{IML1} for fulfilling the required refractive index calculated using (2) and (6), and thus achieving a wideband and low-loss polarizer

C. *Overall Structure Design*

The proposed anisotropic metamaterial unit cell for LP-CP conversion is constructed by stacking IMLs on each side of the core layer in z-axis, as shown in Fig. 11. Table I summarizes the optimized dimensions of the proposed unit cell. A simulation model of the unit cell for the IML was constructed in HFSS to investigate its characteristics (e.g., transmission and reflection coefficients).

Fig. 12 shows the simulated reflection coefficients for two orthogonal polarizations. It can be observed that the reflection coefficients are lower than -10 dB over the frequencies ranging from 7 GHz to 12.3 GHz, while the transmission coefficients are better than -0.25dB. This proved that the IML layer provides an effective antireflection interface between free-space and core layer.

Fig. 13 illustrates the magnitude and phase of the transmitted wave passing through the overall unit cell. Through the observation of this figure, a CP wave can be generated because the magnitude T_x is close to that of T_y while the phase difference between T_x and T_y is 90° at the center frequency of 10 GHz. The stability of the magnitude and phase response over a wide frequency range enables a CP wave to be generated over a similarly wide frequency range.

Based on the calculation of (8), Fig. 14 is provided to demonstrate the simulated electrical length of the polarizer compared with the required electrical length in terms of free-space wavelength. It can be found that the heights of core layer and IML in simulation are close to those in calculation at center frequency (10 GHz), which indicates that (8) can be applied to guide the design of the overall polarizer.

IV. Results And Discussions

To investigate the performance of the complete polarizer design, a 9 x 9 array composed of the proposed metamaterial unit cells is illustrated in Fig. 15. 9 metamaterial unit cells were assembled along the y-axis to form a metamaterial slab, while there are 9 slabs arranged in the x-axis with equal spacings of

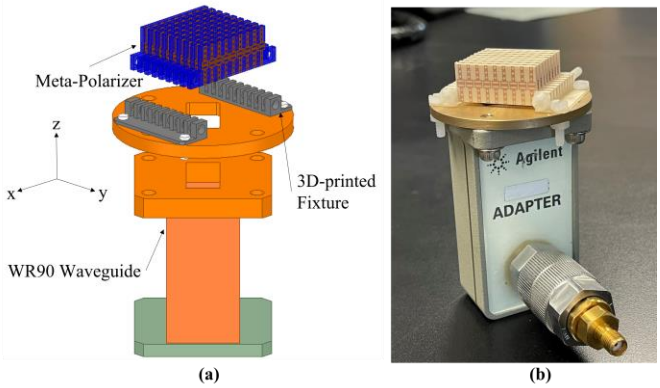

Fig. 16. (a) Simulated model, and (b) fabricated prototype of the proposed CP antenna.

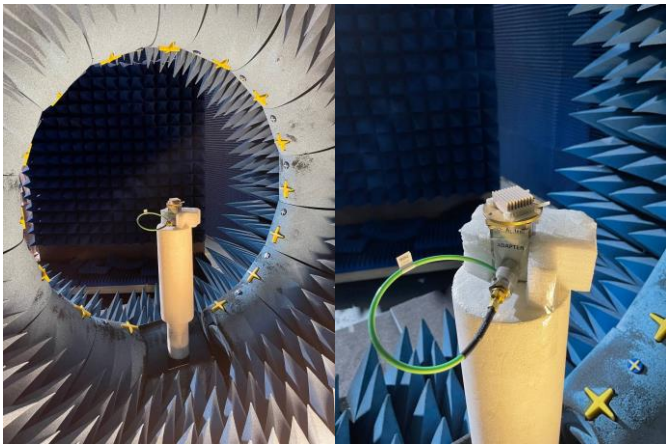

Fig. 17. Measurement Setup of the proposed CP antenna.

T_{air} = 1.5mm (0.5 λ_0 at 10 GHz). The proposed metamaterial was excited by a WR-90 waveguide as shown in Fig. 16. The selection of waveguide antenna as the source is due to the broadband performance and stable radiation characteristics over the frequency range. The LP wave from the waveguide is orientated at 45° to the plane containing the metamaterial slabs. A supporting fixture was made from Polylactic Acid (PLA) by using 3D printer. The supporting structure realized the alignment between the metamaterial-based polarizer and the feeding waveguide. Note that the angle should be -45° for LHCP and 45° for RHCP, respectively.

The performance of the proposed CP antenna was simulated with the aid of HFSS. The measurement of S11 was performed by using an Agilent Network Analyzer (model number: N5230A). The far-field radiation characteristics, including the gain, axial ratio (AR), and radiation pattern, were obtained with the aid of the SATIMO system and presented in Fig. 17.

Fig. 18 depicts the measured reflection coefficients and gains of the proposed CP antenna with and without the polarizer. As observed from the measured results, the impedance bandwidth

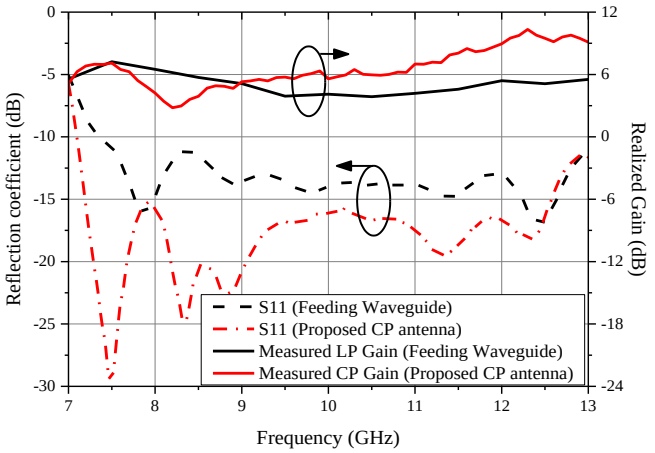

Fig. 18. Measured S-parameters and gains of the proposed CP antenna compared with the feeding waveguide.

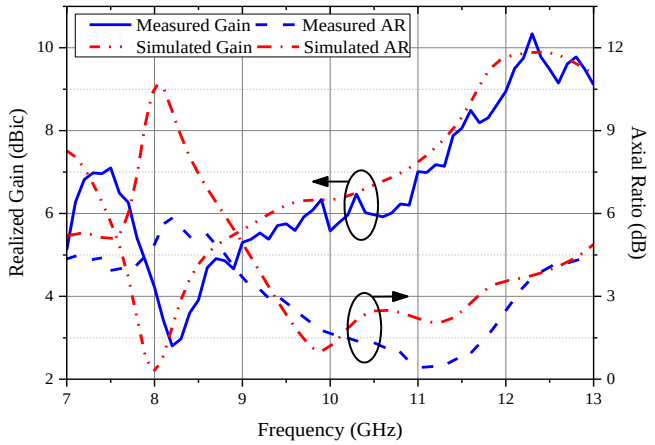

Fig. 19. Simulated and measured axial ratio and gain of the proposed CP antenna.

($S_{11} \leq$ -10 dB) for the proposed CP antenna is 62.4% (7.08 − 13.5GHz). It is indicated that the reflection coefficient with the polarizer included is even lower than that without a polarizer over the entire measured bandwidth due to the combination of core layer and IML. Moreover, the comparison between the measured CP gain of the proposed CP antenna and the measured LP gain of the feeding waveguide shows that the gain of the proposed antenna is 2 dB higher than that of the feeding waveguide. Fig. 19 shows the realized gains and ARs at the broadside direction ($\theta = 0^{\circ}$, and $\varphi = 0^{\circ}$). It can be observed that the measured 3-dB AR bandwidth ranges from 9.25 GHz to 12.5GHz (29.9%) whereas the simulated one is from 9.3 GHz to 11.7 GHz (22.8%). A consistent gain of around 6.5 dBic is obtained over the aforementioned AR bandwidth for both simulated and measured results. The CP gain drops by 2dB at 8.25GHz because the AR reaches 5.85 which makes the antenna approximate to LP radiation at such frequency.

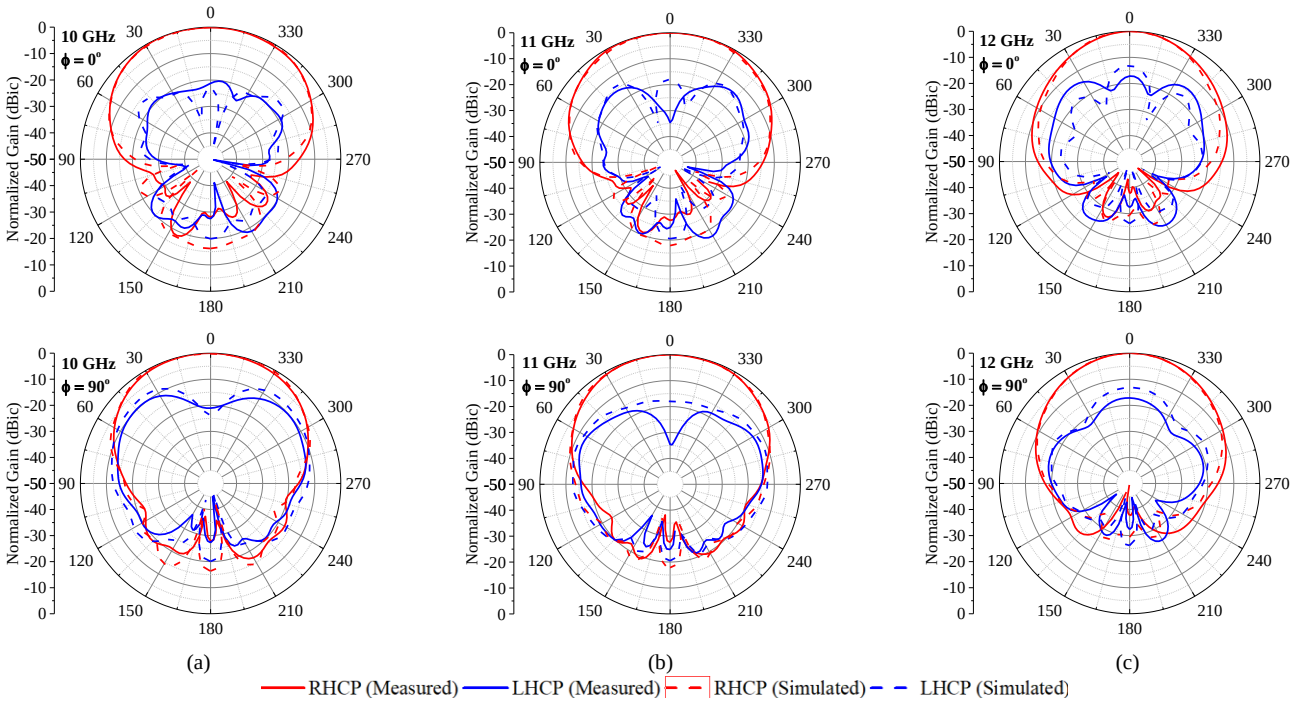

Fig. 20. Measured and simulated radiation patterns of the proposed CP antenna at (a) 10GHz, (b) 11GHz, and (c) 12GHz.

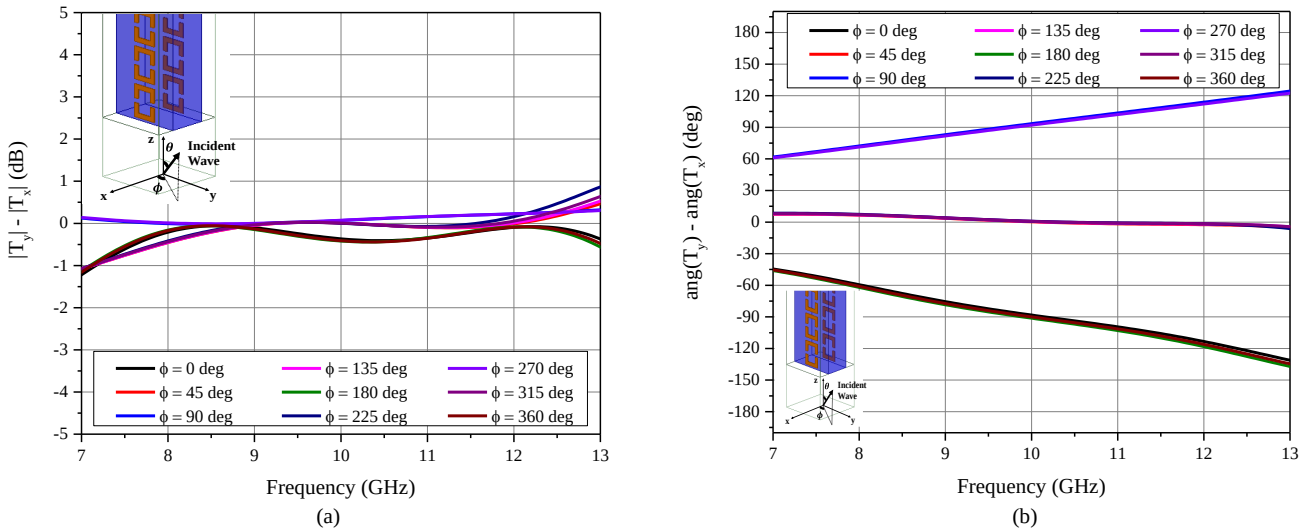

Fig. 21. Transmission (a) magnitude and (b) phase differences between two orthogonal polarizations with the variation of ϕ at $\theta = 45^{\circ}$.

Fig. 20 shows the measured and simulated radiation patterns of the proposed CP antenna at 10 GHz, 11 GHz, and 12 GHz. In both xoz- and yoz-planes, it can be found that RHCP radiation dominates the co-polarization of the proposed antenna at the broadside direction. Moreover, the radiation patterns are symmetric over the operating frequency range. Meanwhile, the cross-polarization levels were lower than -15 dB on the broadside direction, which ensures the purity of the CP wave radiations. However, the cross-polarization level increase in the oblique direction due to the angle sensitivity of the proposed anisotropic metamaterial. As observed from Fig. 21, when the meta unit cell is fed by the incident wave with variation of ϕ, the transmission phase differences change rapidly, and transmission magnitude differences are nearly stable at 0dB within the fluctuation of ±1 dB. The transmission phase differences between orthogonally polarized waves are varying back and forth in the range of -90° to 90° as changing ϕ, which resulted in not only RHCP but also LHCP and LP in the oblique direction. Hence, those LHCP or LP waves eventually result in the higher cross-polarization levels at the directions other than the broadside direction.

V. Conclusion

This paper presents a wideband circularly polarized antenna based on an anisotropic metamaterial. An anisotropic metamaterial unit cell with impedance matching structures was introduced and adopted to construct a CP polarizer. To validate the LP-CP conversion of the proposed design, a prototype of the polarizer assembled with a waveguide was fabricated and

measured. The simulated and measured results are in good agreement and the proposed design possesses a wide impedance bandwidth ($S_{11} \leq$ -10 dB) of 62.4% covering the 3-dB AR bandwidth of 29.9%. The gain of the proposed design is 2 dB higher than that of the feeding waveguide. Moreover, the height of the proposed polarizer is 0.41 λ_0 (where λ_0 is the wavelength at 10.5 GHz).

REFERENCES

[1] M. Akbari, M. Farahani, A. Sebak and T. A. Denidni, "Ka-band linear to circular polarization converter based on multilayer slab with broadband performance," *IEEE Access*, vol. 5, pp. 17927-17937, 2017.

[2] C. Ding and K. -M. Luk, "Low-profile planar dielectric polarizer using high-dielectric-constant material and anisotropic anti-reflection layers," *IEEE Trans. Antennas Propag.*, vol. 69, no. 12, pp. 8494-8502, Dec. 2021.

[3] M. Akbari, S. Gupta, M. Farahani, A. R. Sebak, and T. A. Denidni, ''Analytic study on CP enhancement of millimeter wave DR and patch subarray antennas,'' *Int. J. RF Microw. Comput.-Aided Eng.*, vol. 27, no. 1, pp. 21053, Jan. 2017.

[4] D. Roddy, *Satellite Communications*, 4th ed. New York, NY, USA: McGraw-Hill, 2006.

[5] C. Dietlein, A. Luukanen, Z. B. Popovic, and E. Grossman, "A W-band polarization converter and isolator," *IEEE Trans. Antennas Propag.*, vol. 55, no. 6, pp. 1804–1809, Jun. 2007.

[6] R. Orr, G. Goussetis, V. Fusco, and E. Saenz, "Linear-to-circular polarization reflector with transmission band," *IEEE Trans. Antennas Propag.*, vol. 63, no. 5, pp. 1949-1956, May 2015.

[7] Y. He, W. He and H. Wong, "A wideband circularly polarized cross-dipole antenna," *IEEE Antennas Wireless Propag. Lett.*, vol. 13, pp. 67-70, 2014.

[8] H. Nakano, *Helical and Spiral Antennas*. New York: Research Studies Press, Wiley, 1987.

[9] H. Nakano, K. Nogami, S. Arai, H. Mimaki and J. Yamauchi, "A spiral antenna backed by a conducting plane reflector," *IEEE Trans. Antennas Propag.*, vol. 34, no. 6, pp. 791-796, Jun. 1986.

[10] K. F. Lee, and K. M. Luk, *Microstrip Patch Antennas*, 2nd ed. Singapore: Imperial College Press, 2010, pp. 459-524.

[11] K. W. Leung and H. K. Ng, "Theory and experiment of circularly polarized dielectric resonator antenna with a parasitic patch," *IEEE Trans. Antennas Propag.*, vol. 51, no. 3, pp. 405-412, Mar. 2003.

[12] L. Young, L. A. Robinson, and C. Hacking, "Meander-line polarizer," *IEEE Trans. Antennas Propag.*, vol. 21, no. 3, pp. 376–378, May 1973.

[13] W. Zhang, J. Li, and J. Xie, "A broadband circular polarizer based on cross-shaped composite frequency selective surfaces," *IEEE Trans. Antennas Propag.*, vol. 65, no. 10, pp. 5623-5627, Oct. 2017.

[14] L. Martinez-Lopez, J. Rodriguez-Cuevas, J. I. Martinez-Lopez and A. E. Martynyuk, "A multilayer circular polarizer based on bisected split-ring frequency selective surfaces," *IEEE Antennas Wireless Propag. Lett.*, vol. 13, pp. 153-156, 2014.

[15] K. X. Wang and H. Wong, "A wideband millimeter-wave circularly polarized antenna with 3-D printed polarizer," *IEEE Trans. Antennas Propag.*, vol. 65, no. 3, pp. 1038-1046, Mar. 2017.

[16] S. O. Kasap, "Polarization and Modulation of Light," in Optoelectronics and Photonics: Principles and Practices, 2nd ed. Upper Saddle River, NJ, USA: Pearson, 2013, ch. 6, sec. 6.3, pp. 452 – 455.

[17] T. C. Edwards, and M. B. Steer, *Foundations for Microstrip Circuit Design*. 4th ed. West Sussex, UK: Wiley, 2016, pp. 76-79.

[18] D. R. Smith, D. C. Vier, T. Koschny, and C. M. Soukoulis, "Electromagnetic parameter retrieval from inhomogeneous metamaterials," *Phys. Rev. E, Stat. Phys. Plasmas Fluids Relat. Interdiscip. Top.*, vol. 71, pp. 036617-1–036617-11, Mar. 2005.